Vibrational and electronic spectroscopy of the retro-carotenoid rhodoxanthin in avian plumage, solid-state films, and solution

CrossMark

Christopher J. Berg [a], Amy M. LaFountain [b], Richard O. Prum [c], Harry A. Frank [b], Michael J. Tauber [a],*

[a] Department of Chemistry and Biochemistry, University of California at San Diego, 9500 Gilman Drive MC 0314, La Jolla, CA 92093, USA
[b] Department of Chemistry, University of Connecticut, 55 North Eagleville Road, Storrs, CT 06269, USA
[c] Department of Ecology and Evolutionary Biology, Peabody Museum of Natural History, Yale University, 21 Sachem Street, New Haven, CT 06511, USA

ARTICLE INFO

ABSTRACT

Rhodoxanthin is one of few retro-carotenoids in nature. These chromophores are defined by a pattern of single and double bond alternation that is reversed relative to most carotenoids. Rhodoxanthin is found in the plumage of several families of birds, including fruit doves (*Ptilinopus*, Columbidae) and the red cotingas (*Phoenicircus*, Cotingidae). The coloration associated with the rhodoxanthin-containing plumage of these fruit dove and cotinga species ranges from brilliant red to magenta or purple. In the present study, rhodoxanthin is characterized *in situ* by UV–Vis reflectance and resonance Raman spectroscopy to gain insights into the mechanisms of color-tuning. The spectra are compared with those of the isolated pigment in solution and in thin solid films. Key vibrational signatures are identified for three isomers of rhodoxanthin, primarily in the fingerprint region. Electronic structure (DFT) calculations are employed to describe the normal modes of vibration, and determine characteristic modes of retro-carotenoids. These results are discussed in the context of various mechanisms that change the electronic absorption, including structural distortion of the chromophore or enhanced delocalization of π-electrons in the ground-state. From the spectroscopic evidence, we suggest that the shift in absorption is likely a consequence of perturbations that primarily affect the excited state of the chromophore.

© 2013 Elsevier Inc. All rights reserved.

Introduction

Some of the most vibrant colors of feathers are derived from carotenoids. Colors such as yellow, red, or purple in feathers can be partly attributed to unique carotenoids that are formed metabolically from a small number of dietary carotenoids. The absorption characteristics of these molecules depend in large part upon the length of double-bond conjugation, which can vary substantially. In one remarkable example, 16 different carotenoids were recently identified in the plumage of cotingas, and their double-bond conjugation lengths were found to span all values from 9 to 15, inclusive [1].

Apart from the expected effect that different carotenoids have on coloration, there are also intriguing examples of feathers with the same composition of chromophore(s), yet varied coloration. These cases have long been of interest [2–5] and there are several possible explanations for the variation. First, structural coloration can influence or even dominate the overall color of a feather, independent of the pigments [6–8]. Second, other non-carotenoid pigments, particularly melanin, contribute to the coloration of some

bird feathers [9,10]. Third, the electronic absorption of carotenoids can be tuned by polarizing influences (e.g. hydrogen bonding, or nearby charges) in the keratin environment. These types of specific interactions between the carotenoids and surrounding protein are considered likely causes for substantial color-tuning in various carotenoproteins, e.g. within crustaceans [11,12].

An additional mechanism of color-shifts is based upon electronic interaction between neighboring carotenoid molecules. The mechanism has been considered a possibility for protein-bound astaxanthin in crustaceans [13,14] as well as ketocarotenoids within avian plumage [5]. Electronic interactions between chromophores are of exceptional interest, because several photophysical processes that are not possible for a monomer become available for two or more coupled chromophores. In particular, the process of singlet exciton fission, whereby a singlet exciton forms two triplet excitons on neighboring chromophores, becomes possible for carotenoids [15–20]. Despite the evidence for singlet fission in biological systems with carotenoids, no functional role for the mechanism has been determined. We recently proposed that intermolecular singlet fission may provide a photoprotective advantage for carotenoids, via the partitioning of absorbed photonic energy over two chromophores, rather than a single chromophore [18]. Evidence supporting this idea has yet to be found; nevertheless, our interest in the topic has led us to

investigate natural systems where electronic interaction between carotenoids could play a role in their excited-state dynamics.

The five birds that are the focus of the present study (Fig. 1) all have the carotenoid rhodoxanthin as the principle chromophore in portions of their plumage. The pattern of single/double bond alternation of rhodoxanthin, a retro-carotenoid, is reversed from that found for the vast majority of carotenoids, such as zeaxanthin or β-carotene (Fig. 2). Despite the shared chromophore, the coloration of the feathers probed here varies from crimson red to burgundy, pink, or purple. We considered exciton coupling to be among the possible reasons for the variation. Four of the birds are fruit doves in the genus *Ptilinopus* within the Columbidae family: Wompoo Pigeon (*Ptilinopus magnificus*), Beautiful Fruit Dove (*Ptilinopus pulchellus*), Yellow-bibbed Fruit Dove (*Ptilinopus solomonensis*), and Jambu Fruit Dove (*Ptilinopus jambu*). The presence of rhodoxanthin in this genus has been known for decades [2]. One cotinga species, *Phoenicircus carnifex* (Cotingidae), was also included in our study because the bright red plumage of this bird is also known to contain rhodoxanthin [1,21]. Our principle aim was to gain an understanding of rhodoxanthin *in situ*, both from vibrational and electronic spectroscopy. The combined approach of *in situ* resonance Raman and electronic spectroscopy has been a powerful one for identifying various causes of coloration in carotenoid/protein systems, including structural distortion, π-electron delocalization, and exciton coupling [4,5,11,22,23].

At the outset, the lack of resonance Raman spectra of retro-carotenoids in the literature hampered our exploration of the chromophores in the feathers. One reason for the dearth of spectra is that retro-carotenoids are far less common in nature than carotenoids having the normal pattern of single/double bond alternation [24]. Rhodoxanthin occurs in various plants [25–34], lichens [35], and animals including birds [1–3,21,36–39], and fish [40]. One can infer that vibrational resonance Raman spectra of rhodoxanthin may have been acquired previously [41–43]. However, the
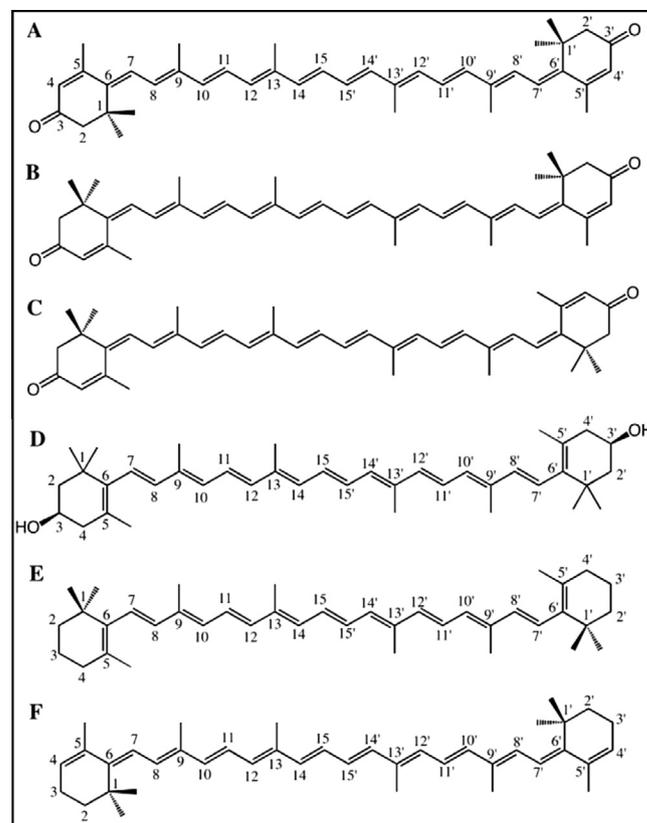
Fig. 2. Chemical structures of (A) (6E,6′E)-rhodoxanthin, (B) (6Z,6′E)-rhodoxanthin, (C) (6Z,6′Z)-rhodoxanthin, (D) (3R,3′R)-zeaxanthin, (E) β-carotene, and (F) (6E,6′E)-isocarotene.

prior reports did not make a clear connection between spectra (or peak positions) and the carotenoid. Infrared spectra or band positions of retro-carotenoids have been reported as part of synthetic efforts [44–47]. However, the analyses of IR spectra of retro-carotenoids are sparse and tend to focus on a small portion of the spectrum [48–50]. To our knowledge, there is only a single example in the literature where a full IR spectrum of rhodoxanthin is illustrated [51].

Given the lack of any comprehensive report or analysis of vibrational spectra of retro-carotenoids, we have explored the resonance Raman spectroscopy of rhodoxanthin within feathers (*in situ*), and as an isolated chromophore, in solution and in thin solid films. The spectra of three isomers of rhodoxanthin are compared with (3R,3′R)-zeaxanthin, which has a well-understood vibrational spectrum [52]. Assignments of the bands of the retro-carotenoid were aided by the results from density functional theory (DFT[1]) calculations. The vibrational spectra of the carotenoids in the feathers, as well as their absorption spectra, are evaluated with the aim of assessing various mechanisms for the different colors of these feathers.

Methods and materials

Pigment extraction and analysis

The feathers of this study were obtained from the University of Kansas Natural History Museum (Lawrence, KS, USA) and the Yale Peabody Museum of Natural History (Yale University, New Haven, CT, USA). The five feather types are described as follows: (1) red
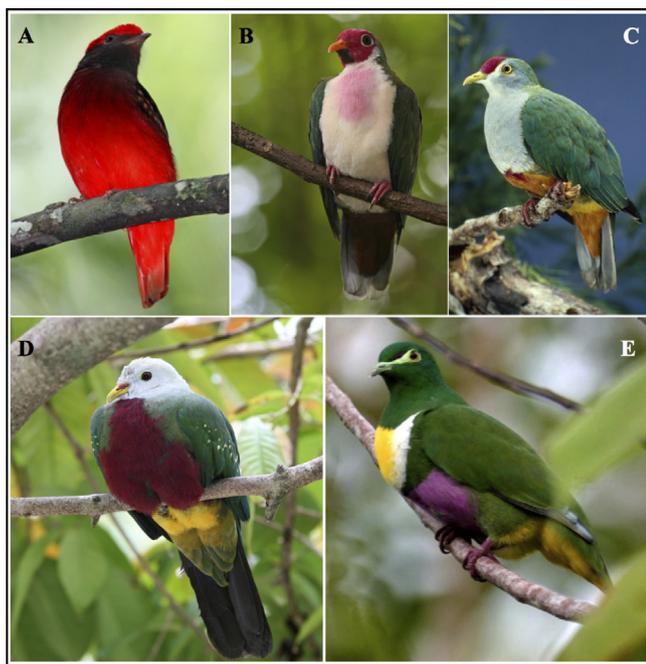
Fig. 1. Photos of bird species with rhodoxanthin in portions of their plumage: (A) Black-necked Cotinga, *Phoenicircus nigricollis* (close relative of *Ph. carnifex*), (B) Jambu fruit dove, *Ptilinopus jambu*, (C) Beautiful fruit dove, *Ptilinopus pulchellus* (D) Wompoo pigeon, *Ptilinopus magnificus* (E) Yellow-bibbed fruit-dove, *Ptilinopus solomonensis*. Photo credits: (A) Wim de Groot; (B and C) T. Friedel/VIREO; (D) W. Peckover/VIREO; (E) Mehd Halaouate.

---

body feathers of a male *Phoenicircus carnifex* (KU 88704, collected March 1997); (2) burgundy breast feathers of a male *Ptilinopus magnificus septentrionalis* (YPM 74482, collected October 1960); (3) crimson breast feathers of a male *Ptilinopus pulchellus pulchellus* (YPM 73164, collected 1955); (4) purple breast feathers of a male *Ptilinopus solomonensis speciosus* (YPM 41523, collected November 1937); and (5) pink breast feathers of a male *Ptilinopus jambu* (YPM 62797, collected October 1952).

The carotenoids were extracted from the feathers via procedures described previously [53,54]. The pigmented sections of cleaned feathers were trimmed, and placed in a glass test tube under acidified pyridine at 90 °C for several hours. The *Pt. solomonensis*, *Pt. magnificus* and *Pt. pulchellus* feathers were each treated in the acidified pyridine for 3 h, after which the *Pt. solomonensis* feathers were white, whereas the feathers of *Pt. magnificus* and *Pt. pulchellus* were dark brown. The treatment of *Pt. jambu* feathers was stopped after 2 h, and they were white at that time. *Ph. carnifex* feathers were pale orange post-extraction. Next, methyl-*tert*-butyl ether (MTBE)/water (3:1 v/v) was added to the test tubes to partition carotenoid pigments from water-soluble lipids. The aqueous phase was removed by pipette, and the MTBE phase was washed twice with additional water. The carotenoid pigments in the MTBE layer were collected and dried, and later analyzed by HPLC and absorption spectroscopy as described previously [1,53]. Briefly, the HPLC protocol utilized a multi-solvent delivery system (Waters 600), a 5 μm silica column (Phenomenex Luna, 250 × 4.6 mm) and a photodiode array detector (Waters 2996). The mobile phase consisted of a linear gradient that began with 10% acetone in hexane and reached 20% acetone in hexane over 40 min. The flow rate was 1.0 mL/min.

Pigments eluting from the HPLC were collected and their absorption spectra recorded in the mobile phase. The pigments from *Pt. magnificus* were sufficiently concentrated for mass spectrometry, which was performed in the APCI mode (Applied Biosystems API 2000). The samples were dissolved in methanol and introduced into the mass spectrometer by direct infusion at a rate of 20 μL/min.

Preparation of rhodoxanthin isomers

Synthetic rhodoxanthin was dissolved in acidified pyridine and heated to a temperature of 90 °C. The sample was analyzed with normal-phase HPLC as described above, and three bands were collected with elution times that were separated by ~1 min intervals. The absorption spectra of the isolated pigments in the mobile phase (not shown) were consistent with their identification as (6E,6′E)-, (6E,6′Z)-, and (6Z,6′Z)-isomers of rhodoxanthin (see below) [29].

Preparation of thin-films

Three thin-films of (6E,6′E)-, (6E,6′Z)-, and (6Z,6′Z)-rhodoxanthin were prepared from the synthetic rhodoxanthin treated with acidified pyridine. The dried rhodoxanthin was dissolved in acetone and added drop-wise to a glass microscope slide, with sufficient time between each drop to allow the solvent to evaporate.

Optical microscopy

Images of the five rhodoxanthin-containing feathers were acquired with a CCD camera (AVT Stingray F-201B/C) attached to an upright microscope (Zeiss Axio Imager). The feathers were epi-illuminated with light from a quartz tungsten halogen lamp. The objective was a NA = 0.25 plan semi-apochromat (Zeiss Epiplan-Neofluar 10×). A diffuse white reflector (Spectralon) was used to perform a color balance calibration. After the calibration, each feather was placed on the Spectralon block for acquiring an image.

Spectroscopy

Absorption spectroscopy

UV–Vis absorption spectra of the chromophores in solution were measured with a scanning spectrometer (Shimadzu UV-3600). Solutions were held in a quartz cuvette with 1 cm path length, unless otherwise noted.

Diffuse reflectance and forward-scattering spectroscopy

Back-scattered and forward scattered light from the five plumage samples were recorded in configurations that are the same as those normally employed for measurement of diffuse reflectance and diffuse transmittance spectra (See Fig. S1). A UV–Vis spectrophotometer with integrating sphere attachment (Shimadzu UV-3600, ISR-3100) was employed. Prior to measurements of the samples, a baseline correction was performed with a barium sulfate white-light reflector positioned at an appropriate port of the integrating sphere. Each feather was positioned in the beam, and covered by a mask with 3.0 mm open diameter so that the most colorful region was probed. We note that the feathers have ~50% open area between barbs or barbules, thus considerable light passes through the feathers unimpeded and is also not captured by the integrating sphere. Also, forward scattering and glancing reflection from the barbs are expected to dominate in the (nominally) transmittance measurement.

Macro-Raman spectroscopy

514.5 and 568.2 nm excitation beams were generated by an argon/krypton ion laser (Laser Innovations, Innova-70C). The beam was directed through a narrow-band interference filter (Semrock) that matched the wavelength of the laser line.

For the solid-state samples (feathers, thin films), Raman scattered light was collected in a 180-degree back-scattering geometry. A 75 mm cylindrical lens was used to focus the laser beam along one axis. At the sample, the beam had an elliptical profile, with axis lengths 2.50 × 0.040 mm. The low excitation power (<1.5 mW and ~3.3 mW) kept the irradiance at the sample to 2 W/cm² (for feathers) and 4 W/cm² (for thin films) or less. For solution-phase experiments, the sample was held in a 10 × 4 mm septum-capped quartz cuvette with clear bottom window. The rhodoxanthin solution was purged and agitated during the Raman collection with a slow stream of nitrogen gas. The rhodoxanthin isomers were each dissolved in dimethyl sulfoxide (DMSO). DMSO was selected in part because the solvent has a relatively high boiling point (189 °C), therefore purging resulted in little evaporation during the course of the experiment. A 75 mm cylindrical lens was used to focus the beam along one axis, and the dimensions at the sample were approximately 1.25 × 0.040 mm. The excitation power was approximately 4.5 mW, and the irradiance was ~10 W/cm². Raman scattered light was collected at 90° relative to the propagation of the excitation beam.

The detection setup for the macro-Raman experiments employed an F/1.2 collection lens (Canon FD, focal length 85 mm). An F/4 achromatic lens was used to focus the scattered light onto the entrance slit of a 320 mm focal length spectrograph (Horiba Jobin–Yvon, iHr-320). The scattered light also passed through a polarization scrambler and an edge filter (cutoff either 514.5 or 568.2 nm; Semrock, Razoredge) prior to the entrance slit. The spectrograph was equipped with 1200 and 2400 groove/mm holographic gratings, and an open-electrode CCD detector (Horiba Jobin–Yvon Synapse).

Micro-Raman spectroscopy

The same laser source, filters, and spectrograph were utilized as for the macro-Raman experiments. The beam was directed into a Zeiss Axio-Imager upright microscope modified with beamsplitters

appropriate for routing the laser beam to the objective, and for transmitting the Raman-scattered light efficiently. The excitation beam was focused onto the sample with a 0.55 NA objective lens (Zeiss LD EC Epiplan-Neofluar 50×). The diameter of the laser beam at the sample was approximately 1 μm. The average power of the excitation beam was kept below 50 μW (for thin films) and 200 μW (for feathers), which correspond to irradiance levels of 6000 and 30,000 W/cm^2, respectively. The typical irradiance at the sample for the micro-Raman experiments was a factor of 10^3 or 10^4 higher than for macro-Raman experiments. Scattered light was collected with the same objective lens, and subsequently directed along a path that included a polarization scrambler and an edge filter that was selected for the excitation wavelength. The scattered light was then focused at the spectrograph slit with an achromatic lens (focal length 125 mm).

Low-temperature micro-resonance Raman spectroscopy

A Linkam THMS600 microscope stage was employed to cool samples to nearly the boiling temperature of liquid nitrogen (−196 °C). A barb was cut from feather samples and placed between two glass coverslips. Thin layers of silicone oil were used to hold the sample in place, and to allow thermal conduction between the sandwich assembly and the cold block. An internal probe indicated a temperature of −195 °C. It was not certain that the feather samples reached the low temperature of the substrate; however, a vacuum was pulled on the sample space during the Raman spectroscopy to minimize any temperature gradient. For the low temperature resonance Raman studies of the thin film of (6Z,6′Z) rhodoxanthin, the microscope slide was placed inside a Linkam LTS420 cooling stage and subsequently cooled until the temperature probe in the cold block read −195 °C. Excitation powers were less than 300 μW for all low-temperature micro-Raman experiments.

The experimental conditions for all macro- and micro-Raman experiments are summarized in Table S1. A 2400 groove/mm grating was employed for acquisition of most macro- and micro-Raman spectra. One exception was the solution-phase macro-Raman experiments, where the 1200 groove/mm grating was used. Slit-widths were selected between 0.030 and 0.100 mm, depending upon the need for resolution or system throughput. The spectral resolution was approximately 3 (6) cm^{-1} with the 2400 (1200) groove/mm grating and 0.050 mm slit width.

Calculations

Electronic structures and geometry optimizations were performed for (6E,6′E)-, (6E,6′Z)-, and (6Z,6′Z)-rhodoxanthin, as well as β-carotene and a model retro-carotenoid isocarotene. The method was density functional theory (DFT) with B3LYP functional, and a 6–31G(d) basis set. The software was Gaussian 09W [55]. Initial structures were drawn with ChemDraw, optimized with the Hartree–Fock method, and subsequently optimized with DFT. A normal mode analysis was done at the optimized geometry. The harmonic frequencies were subsequently scaled by a factor of 0.9614 [56], which gave good agreement between the calculated and experimental frequencies.

Results and discussion

Pigment extraction and analysis

Extraction of the carotenoids from *Pt. magnificus* feathers yielded a deep red solution. HPLC analysis (Fig. 3) showed three major peaks with retention times of 10.0, 11.3, and 12.2 min. These retention times, along with the absorption spectra in the mobile
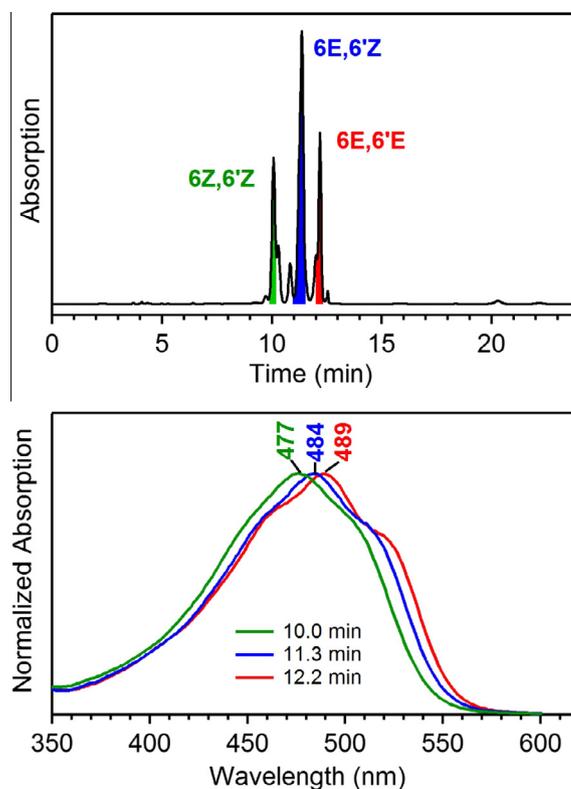
Fig. 3. (Top) Normal-phase HPLC chromatogram of *Pt. magnificus* feather extract, with detection at 480 nm. (Bottom) Absorption spectra corresponding to the three major bands colored in the top panel. The absorption of each eluted band was measured while in the mobile phase solvent, which is 12–13% acetone in hexane (see text for details).

phase solvent, matched those found upon analysis of the heated sample of synthetic rhodoxanthin. The peaks eluting at 11.3 and 12.2 min were analyzed by mass spectrometry and both were found to have a mass of 562 m/z, consistent with rhodoxanthin. Therefore, it can be concluded that the red coloration of the breast feathers of *Pt. magnificus* arises from the retro-carotenoid rhodoxanthin, which is consistent with previous findings by Völker [2].

The λ_{max} positions for the three bands of the *Pt. magnificus* extract in the HPLC mobile phase solvent (12–13% acetone in hexane) are 477, 484, and 489 nm (Fig. 3). After drying and re-dissolving the pigment in methanol, the spectra (not shown) have almost no resolved vibronic features, and the maxima are located at 485, 490, and 497 nm. These positions are not in quantitative agreement with *circa* 10 nm spacing between neighboring maxima that have been reported elsewhere [24]. However, the λ_{max} positions and the spectra of Fig. 3 are in good agreement with those reported for rhodoxanthin isomers isolated from gymnosperms [29]. In order of increasing wavelength for λ_{max}, the isomers are 6-*cis*, 6′-*cis* (6Z,6′Z); 6-*trans*, 6′-*cis* (6E,6′Z); and 6-*trans*, 6′-*trans* (6E,6′E) rhodoxanthin. It is important to note that isomerization of the carotenoid is a likely consequence of the extraction procedure, because elevated temperatures were employed. Therefore it is not possible to infer the isomeric content of the feathers from the HPLC analysis reported here.

The HPLC chromatograms of extracts from *Pt. solomonensis*, *Pt. jambu*, and *Pt. pulchellus* feathers revealed three bands which eluted with retention times and displayed absorption spectra that were similar to those found for extracts of burgundy *Pt. magnificus* feathers. HPLC chromatograms of the *Ph. carnifex* extract yielded the same three peaks, plus an additional one at 27 min which was verified by mass spectrometry to be all-*trans* lutein (data not

shown). However, the amount of lutein is estimated to be less than 5% of total carotenoid in the feather [1]. Therefore, we conclude that the dominant pigment in all of these feathers is rhodoxanthin.

While the above focuses on the extracted chromophores, our procedure did not extract a brown pigment that remained in the feathers of *Pt. magnificus* and *Pt. pulchellus*. Based on prior reports, it is likely that the brown color is caused by eumelanin [9,10]. Additionally, *Ph. carnifex* feathers remained a pale orange after the extraction, which may indicate the presence of pheomelanin [9,10]. The purple feathers of *Pt. solomonensis* and the pink feathers of *Pt. jambu* both appeared colorless following extraction, and we conclude that the melanin content in these feathers is insignificant.

Optical microscopy

The ranking of the feather barbs from the strongest red to strongest purple coloration in the optical images (Fig. 4) were *Pt. magnificus* = *Ph. carnifex*, *Pt. pulchellus*, *Pt. jambu*, *Pt. solomonensis*. The regions of the feather barbs with the strongest red or purple coloration were probed by Raman spectroscopy. The probed regions were generally the barbules, except in the case of *Ph. carnifex*, which has significant concentration of carotenoids in the central shafts (rami) of its barbs. The images of Fig. 4 also show several characteristics that were not investigated in depth. First, the rami of *Pt. pulchellus* and *Pt. magnificus* are dark; thus melanin may be more concentrated in this region than in the barbules. Second, several feather types have some iridescence. The effect gives the barbs of *Pt. magnificus* a green or purple hue. Some barbules of *Pt. solomonensis* and of *Pt. pulchellus* appear to be weakly iridescent as well. The iridescent regions of the feathers in the present study were avoided in the Raman measurements. Third, the breast feathers of several birds exhibit a color gradient from the base of the ramus to the tip. For *Pt. magnificus*, the color varies from iridescent green to red; for *Pt. pulchellus*, yellow to bright crimson. Only the reddest regions of these feathers were probed in the present study.
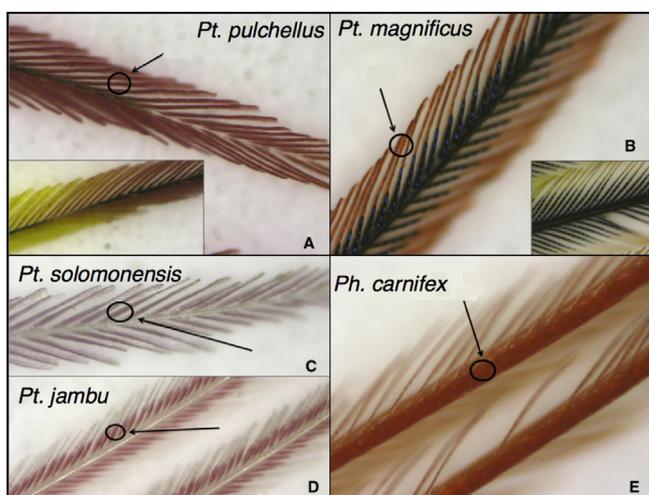
Fig. 4. Images of feather barbs by optical microscopy. Circles indicate the approximate areas probed with resonance Raman spectroscopy. These regions were selected for the deepest coloration and least iridescence. (A) *Pt. pulchellus*; the inset shows a section of feather barb where a gradient of yellow-to-red color is apparent. (B) *Pt. magnificus*; the inset illustrates that some barbules (not probed) have very little rhodoxanthin, and these were also relatively iridescent. (C) *Pt. solomonensis* (D) *Pt. jambu*; approximately half of each barbule is pigmented with rhodoxanthin (E) *Ph. carnifex*; the ramus of this barb was probed because its color is darker than that of the barbule.

Scattering spectroscopy

The diffuse back-scattering (or diffuse back-reflectance) spectra of the five rhodoxanthin-containing feathers were acquired (Fig. 5). These spectra were compared with diffuse transmittance measurements, which are expected to be dominated by light from glancing reflections and scattering off the various structures of the barbs, rather than transmission through the material structure itself. The same portion of each feather was probed in both measurements. The diffuse back-reflectance and forward-scattering spectra for each sample are similar, although there are differences such as the amount of attenuation in the UV region relative to the visible. It is not fully understood what causes the differences between measurement types.

Absorption by rhodoxanthin causes the diffuse reflectance to drop in the range 400–650 nm. The onset of visible absorption on the low-energy (long-wavelength) side is commonly characterized by a reflectance midpoint, $\lambda(R_{mid})$. The $\lambda(R_{mid})$ value is the wavelength position where the reflectance is midway between a maximum value R_{max} (typically located in the red), and a minimum value R_{min} (in the present case, R_{min} can be found in the region 450–600 nm):

$$\lambda(R_{mid}) = \lambda((R_{min} + R_{max})/2) \qquad (1)$$

We note that the reflectance spectra of *Pt. magnificus* and *Pt. pulchellus* feathers increase monotonically in the red region. This characteristic prevents an accurate selection of R_{max} in Eq. (1), and the reflectance value at 725 nm is used for these feathers. The $\lambda(R_{mid})$ values for both back- and forward- scattering measurements are listed in Table 1.

The characterization of feather pigments by a single parameter $\lambda(R_{mid})$ has general shortcomings, aside from the specific ambiguity
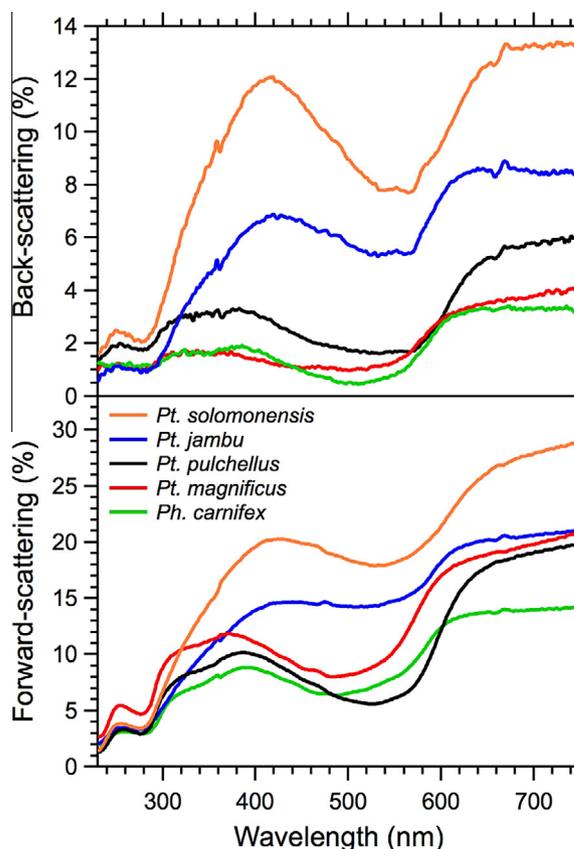
Fig. 5. (Top) Diffuse back-scattering (or diffuse back-reflectance) spectra. (Bottom) Diffuse forward-scattering spectra of the five feathers.

Table 1
Summary of wavelengths that characterize the diffuse back- and forward-scattering spectra, and derived absorption spectra (see text). $\lambda(R_{mid})$ is the wavelength for which the reflectance is midway between a maximum and minimum value. $\lambda(A_{hm})_{avg}$ is the average of the two half-maxima positions $\lambda(A_{hm1})$ and $\lambda(A_{hm2})$ of the derived absorption spectra.

Feather	Back-scattering/back-reflectance				Forward-scattering[a]			
	$\lambda(R_{mid})$ (nm)	$\lambda(A_{hm1})$ (nm)	$\lambda(A_{hm2})$ (nm)	$\lambda(A_{hm})_{avg}$ (nm)	$\lambda(R_{mid})$ (nm)	$\lambda(A_{hm1})$ (nm)	$\lambda(A_{hm2})$ (nm)	$\lambda(A_{hm})_{avg}$ (nm)
Pt. magnificus	584	411	571	**491**	577	430	565	**498**
Ph. carnifex	583	452	567	**510**	580	436	575	**506**
Pt. pulchellus	611	446	602	**524**	602	453	590	**522**
Pt. jambu	594	464	587	**526**	593	457	592	**526**
Pt. solomonensis	614	474	608	**541**	615	465	607	**536**

[a] Forward scattering includes light that is scattered and reflected off of the edges of barbs/barbules, and likely only a small proportion is transmitted through the material structure of the feathers.

noted above for *Pt. magnificus* and *Pt. pulchellus*. For example, it is expected that as pigments reach concentration levels where the reflection approaches low values (i.e., saturation), $\lambda(R_{mid})$ values can shift significantly as a function of concentration. The saturation effect has been discussed previously [57,58]. An improved method of characterizing a pigment within a feather would be the acquisition of its full absorption spectrum *in situ*. We attempted to derive an absorption spectrum of each feather by using the Kubelka–Munk approach with a pile of plates model [59]. The approach was unsuccessful, likely because of significant open spaces in the feathers, edge effects, as well as the opacity of the barbs and barbules. Instead, an attenuation coefficient profile was calculated from the negative log of diffuse reflectance or forward-scattering spectra using:

$$A(\lambda) = -\log(R(\lambda)) \qquad (2)$$

where $A(\lambda)$ is the attenuation coefficient, and $R(\lambda)$ is the fraction of diffuse scattering or reflectance (Fig. 6 and Table 1).

The attenuation coefficient profiles (inset of Fig. 6) show a clear band in the spectral region 400–650 nm that is attributed to absorption by rhodoxanthin. The absorption maximum at ~280 nm can be attributed to the keratin matrix that is the main constituent of the feathers [60]. Carotenoids also absorb in the UV region, as a result of an $S_0 \rightarrow S_n$ transition. However, the molar absorption coefficient of the ~280 nm band for a carotenoid is typically ~5-fold smaller than its primary visible ($S_0 \rightarrow S_2$) absorption band. Therefore, the absorption at 280 nm caused by the carotenoid is expected to be much smaller than that of keratin. Melanin may also contribute to the absorption of *Pt. magnificus* and *Pt. pulchellus*. The absorption of melanin is strongest in the UV region, and the cross section declines monotonically as wavelength increases [61].

The calculated attenuation profiles yield some insights into the relative concentrations of carotenoid within the feathers. We assume equal concentration of keratin and amplitude of the 280 nm band for all five feathers. A comparison of the relative amplitude of the carotenoid and keratin absorption bands across the five spectra suggests that *Pt. pulchellus*, *Ph. carnifex*, and *Pt. magnificus* have 2–3 times greater concentration of carotenoids than *Pt. solomonensis* or *Pt. jambu*. This result is consistent with the muted appearance of *Pt. solomonensis* and *Pt. jambu*.

The carotenoid absorption in the visible region is isolated from the overall attenuation spectrum by fitting a polynomial to spectral regions where that absorption is expected to be at or near baseline. The function is subtracted to remove contributions from scattering or absorption by keratin and melanin. The baseline-subtracted absorption spectra are shown in Fig. 6. The wavelength position of the primary visible absorption is quantified by the average of the wavelength positions for the two half-maxima, $\lambda(A_{hm1})$ and $\lambda(A_{hm2})$ that characterize this band, or $\lambda(A_{hm})_{avg}$. Specifically,

Fig. 6. (Inset) Attenuation coefficient spectra of the five feathers, determined from diffuse forward-scattering data (lower panel of Fig. 5) and Eq. (2) of the text. The spectra are offset for clarity, and no baselines are removed. (Main panel) Derived absorption spectra of rhodoxanthin in the visible region, isolated from the attenuation coefficient spectra of the inset by subtracting a baseline. Spectra are normalized and offset for clarity. The wavelength corresponding to the average of the two half-maxima of each spectrum, $\lambda(A_{hm})_{avg}$, is indicated.

$$\lambda(A_{hm})_{avg} = \left(\frac{\lambda(A_{hm1}) + \lambda(A_{hm2})}{2} \right) \qquad (3)$$

The relevant wavelength positions for each feather are indicated in Table 1. The $\lambda(A_{hm})_{avg}$ values increase in the order *Pt. magnificus*, *Ph. carnifex*, *Pt. pulchellus*, *Pt. jambu*, and *Pt. solomonensis*. The difference between the $\lambda(A_{hm})_{avg}$ values determined from back-scattering and forward scattering spectra are less than 4 nm on average, with a maximum 7 nm difference for *Pt. magnificus*. The relatively small differences found between each pair of measurements provide some assurance that the absorption is assessed reliably with the integrating sphere.

Relationship between UV–Vis absorption and perceived color

The positions of average half-absorption, $\lambda(A_{hm})_{avg}$, span a 38 nm range (~1400 cm^{-1}). The feathers with the strongest red appearance (*Ph. carnifex* and *Pt. magnificus*) have their average

half-absorption located closest to 500 nm. The relatively pure red reflection may occur because absorption by rhodoxanthin in these feathers covers both blue and green spectral regions. In contrast, the feathers with strongest purple or magenta coloration have their average half-absorption centered between 520 and 540 nm. It is well known that when pure green light is subtracted from the white-light sum of red, green and blue, the result is the (non-spectral) color magenta (blue and red). Thus, it is possible that the distinct purple/magenta appearance of *Pt. pulchellus*, *Pt. jambu*, and *Pt. solomonensis* is caused by substantial blue reflection (weaker blue absorption), which in turn results from the relatively bathochromic absorption by rhodoxanthin in these feathers.

It is tempting to attribute the main cause of color variation to the tuning of the absorption band of rhodoxanthin, but other factors could significantly influence the perceived color. First, eumelanin in the plumage of *Pt. magnificus* and *Pt. pulchellus*, or pheomelanin in *Ph. carnifex*, could contribute to the absorption (low reflectance) in the violet-blue spectral region ∼380–500 nm (Fig. 5). The effect would be similar to a blue-shifted absorption by rhodoxanthin. In contrast, the relatively strong violet–blue reflectance of the feathers without melanin, *Pt. solomonensis* and *Pt. jambu*, could contribute to the magenta color of these species. We were unable to assess the relative importance of melanin, versus shifts in the absorption band of rhodoxanthin, to the overall red/purple coloration. Second, as noted above, iridescence was apparent in the microscope images of *Pt. magnificus*, *P. puchellus*, and *Pt. solomonensis* feathers, and could influence their color. Previous studies have shown that while the green coloration of *Ptilinopus* plumage has a structural basis, the distinct red or purple coloration does not [62,63]. The prior work suggests that iridescence does not play an important role in the feathers of our study. Third, the effect of pigment concentration on the plumage coloration was not explored in the present work, although it is clear that there is substantial variation in concentration within the feathers.

Resonance Raman spectrum of (6E,6′E)-rhodoxanthin versus (3R,3′R)-zeaxanthin

Experimental Resonance Raman spectra of (6E,6′E)-rhodoxanthin in DMSO, (3R,3′R)-zeaxanthin in ethanol, and calculated Raman spectra are compared in Fig. 7. The comparison of this particular pair of xanthophylls by experiment and computation is useful because the resonance Raman spectrum of zeaxanthin [52] is nearly identical to that of β-carotene, and is therefore well-understood from extensive prior studies [64–67]. The spectra of rhodoxanthin and zeaxanthin are generally similar. The strongest band of zeaxanthin is denoted ν_1, with maximum near 1525 cm^{-1}. The band results from symmetric linear combinations of several C=C stretches. The ν_1 band of (6E,6′E)-rhodoxanthin is downshifted ∼5 cm^{-1} relative to that of zeaxanthin. Normal mode analysis reveals that the ν_1 mode of retro-carotenoids is unusually extended along the polyene chain, with contributions from all double bonds between C8=C9 and C8′=C9′, inclusive (Table 2, Table S2A and B). By contrast, the ν_1 mode of β-carotene and zeaxanthin is much more localized, with contributions primarily from the double bonds C13=C14 and C13′=C14′.

The fingerprint region (1100–1400 cm^{-1}) of the experimental spectra is dominated by the ν_2 band, with nearly coincident maxima located at 1157–1158 cm^{-1} for both molecules. Despite the matching frequencies, the carbons with the most motion are different: in the case of zeaxanthin, most of the C–C motion is localized to C10–C11, C10′–C11′, C14–C15, and C14′–C15′. For (6E,6′E)-rhodoxanthin the motion is largely with C11–C12, C11′–C12′ and C15–C15′ (Table 2, Table S2A and B). There are a greater number of resonantly enhanced bands in the fingerprint region for rhodoxanthin, including ones centered at ∼1135 cm^{-1} (shoulder), 1283 cm^{-1}, and
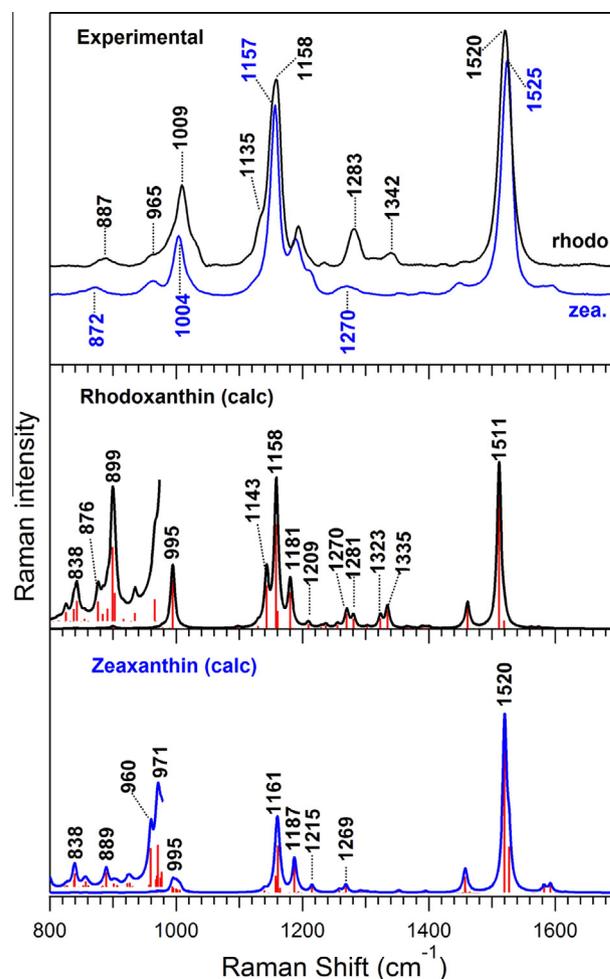
Fig. 7. (Upper panel) Experimental resonance Raman spectra of (6E, 6′E)-rhodoxanthin in DMSO (568.2 nm excitation) and (3R,3′R)-zeaxanthin in ethanol (488.0 nm excitation). (Middle panel) Calculated Raman spectrum of (6E,6′E)-rhodoxanthin. (Lower panel) Calculated Raman spectrum of (3R,3′R)-zeaxanthin. The frequency axes of the calculated spectra are scaled by 0.9614. The 800–980 cm^{-1} region is magnified by 50×. The intensities of the calculated spectra do not take into account any mechanism for resonance enhancement, and are therefore not expected to match the intensities of experimental resonance Raman spectra.

1342 cm^{-1}. The computed normal modes indicate that their motion consists largely of C–C single bond stretches, in combination with C–H rocking (in-plane bending) motions. The calculation of (6E,6′E)-rhodoxanthin also predicts bands at or near the frequencies of experimental ones, e.g. with bands centered at 1143, 1281, and 1335 cm^{-1}. It should be noted that the calculations do not take into account any mechanisms for resonance enhancement, therefore a match with experimental intensities is not expected. Another strong band in the experimental spectra is ν_3, which results largely from methyl rocking motions. The 1009 cm^{-1} frequency for rhodoxanthin is slightly upshifted relative to 1004 cm^{-1} for zeaxanthin. The DFT calculations predict that (6E,6′E)-rhodoxanthin has one main methyl rocking mode, and therefore a simpler band pattern in the ν_3 region, than zeaxanthin. Next, the bands assigned to hydrogen-out-of-plane (HOOP) wagging modes are found in the region 800–1000 cm^{-1}. These bands gain intensity upon loss of planarity of the carotenoid [68,69]. One band near 965 cm^{-1} appears to be centered at nearly the same frequency for both molecules. However another band at ∼887 cm^{-1} for rhodoxanthin is significantly shifted relative to the nearest band of zeaxanthin, which is centered at 872 cm^{-1}. The differences in HOOP wag frequencies

Table 2
Calculated frequencies of select normal modes of (3R,3′R)-zeaxanthin and three isomers of rhodoxanthin.

Frequency of mode (cm^{-1})				Assignment[a]
Zea	(6E,6′E)-rhodo	(6E,6′Z)-rhodo	(6Z,6′Z)-rhodo	
1520				Symmetric C=C stretches, primarily C13=C14
	1511	1513	1516	Symmetric C=C stretches, extending from C8=C9 to C8′=C9′
	1390, 1401	1387, 1395	1386, 1395	Methyl bends + CH rock
	1335[b]	1334	1334	C13–C14 stretch + CH rocks
	1323[b]	1324	–	CH rocks (including ring C4H) for E configuration
	–	1300	1300	CH rocks (including ring C4H) for Z configuration
	1281[b]	1281	1281	CH rocks C14H, C15H
	1270[b]	1270	1270	CH rocks C11H, C14H, C15H
1269[b]				CH rocks C10H, C11H CH(ring)
1215				C14–C15 stretch + CH rocks
	1209	1209	1209	C15–C15′ stretch + CH rocks
	–	1194	1194 (w)	C7–C8 stretch + ring methylene rock + CH rocks
1187				C8–C9 stretches + CH rocks
	1181	1182, 1181, 1177	1178	C7–C8, C11–C12 stretches + CH rocks
1161				C10–C11, C14–C15 stretches + CH rocks
	1158	1152, 1157, 1160	1155	C11–C12, C15–C15′ stretches + CH rocks
	1143[b]	1141	1138 (w)	C15–C15′ stretch + CH rocks
995	995	996, 997	998	Methyl rocks
971				C7H, C8H, C10H, C11H, C12H HOOP wags
960				C7H, C8H, C10H, C11H, C12H HOOP wags
	966	967 (w)	968 (w)	C10H, C11H, C12H HOOP wags
	899[b]	902, 897	902	C7H, C8H and other HOOP wags; ring torsion
889[b]				C10H, C11H, C12H HOOP wags
	884	885, 883	885	C7H, C8H HOOP wags
	876	877	–	C7H and ring CH HOOP wags
838	838	832	833 (w)	C8H, C10H, C11H, C14H, and C15H HOOP wags

Abbreviations: Zea = (3R,3′R)-zeaxanthin; rhodo = rhodoxanthin; HOOP = Hydrogen-out-of-plane; (w) = weak.
[a] A majority of the modes in this list include motion of the unlisted primed carbons on the opposite side of the molecule, e.g. a C13–C14 stretch also implies C13′–C14′.
[b] These modes appear to be the most prominent ones that distinguish the experimental Raman spectra of (6E,6′E)-rhodoxanthin and zeaxanthin.

between the two molecules may be caused by CH out-of-plane motion at the conjugated C4/C4′ carbons of rhodoxanthin. Descriptions and frequencies of the calculated modes that distinguish (3R,3′R)-zeaxanthin and (6E,6′E)-rhodoxanthin are highlighted in Table 2 (see also Table S2A and B).

Differences between computed spectra of (6E,6′E)-isocarotene, and β-carotene

Additional DFT/normal mode calculations of the retro-carotenoid, (6E,6′E)-isocarotene, and β-carotene (Fig. S2, Tables S3 and S4) suggest that the differences described above between rhodoxanthin and zeaxanthin are not limited to these xanthophylls. In brief, the main ethylenic vibration of isocarotene is calculated to be much more delocalized, and the frequency is downshifted 8 cm^{-1}, relative to that of β-carotene. The calculations also show considerably more activity in the fingerprint region of isocarotene, including a band at 1143 cm^{-1}, as well as pairs of bands at 1270/1280 cm^{-1} and 1325/1333 cm^{-1}. These results match those of (6E,6′E)-rhodoxanthin. The calculated spectrum of isocarotene reveals the simplified structure in the ν_3 region, as seen for rhodoxanthin. In the HOOP region, the comparison of isocarotene with β-carotene reflects the same differences as for rhodoxanthin vs. zeaxanthin. The comparisons of the two carotenes and the two xanthophylls indicate that the retro-configuration, rather than any other factor, cause the primary spectral differences in the resonance Raman spectra.

Resonance Raman spectra of rhodoxanthin isomers in solution

The spectra of the three rhodoxanthin isomers in DMSO with 568.2 nm excitation are compared in Fig. 8. Absorption spectra (Fig. S3) were taken before and after exposure to the laser, and no shifts in the absorption maxima for any of the 3 isomers were observed. This result indicates that the majority of each rhodoxanthin

isomer remains in its starting configuration. The position of the ν_1 band maximum is slightly lower in frequency for the *trans* (E) configuration, relative to the *cis* (Z): (6Z,6′Z), 1526 cm^{-1}; (6E,6′Z), 1524 cm^{-1}; and (6E,6′E), 1520 cm^{-1}. The maximum for ν_2 is within the range 1158–1160 cm^{-1} for all isomers, and the variation is neither significant nor systematic among the isomers. In terms of intensities of various bands relative to the ν_1 ethylenic, those centered at 1010 (ν_3), 1195, 1285, and 1343 cm^{-1} increase for the series (6Z,6′Z) → (6E,6′E). For the same series, intensities decrease for bands centered at 825, 1205, 1312, and 1392 cm^{-1}. Peak positions of the ν_1, ν_2, and ν_3 modes for the three isomers in DMSO are listed in Table S5.

The results from normal mode calculations of the three rhodoxanthin isomers are shown in Fig. 9 and Table 2. The DFT calculations agree with experimentally observed downshift of the ν_1 frequency for the *trans* (E) configuration, with calculated ν_1 frequencies of 1516, 1513, and 1511 cm^{-1} for the 6Z6′Z, 6E6′Z, and 6E6′E isomers, respectively. The downshift correlates with enhanced planarity of the polyene backbone including the conjugated rings of rhodoxanthin. With the E-configuration, the dimethyl substituents attached to C1/C1′ straddle the polyene hydrogen attached to the C8/C8′ position, and thus keep the conjugated double bonds of the rings relatively coplanar with the polyene backbone. Conversely, for the Z-configuration there is steric hindrance between the single methyl group attached to C5/C5′, and the hydrogen at the C8/C8′ position. Therefore one would expect a greater dihedral angle between the C=C double bond of each ring and polyene backbone in the Z-configuration versus the E-configuration. The DFT-optimized structure (Table 3) of the (6Z,6′Z) isomer has dihedral angles with magnitude 160.1°; the (6E,6′Z) isomer has dihedral angles 160.1° (Z) and 176.8° (E); and the (6E,6′E) isomer has dihedral angles of 179.9°. Compared to normal carotenoids, the ring end groups of retro-carotenoids are generally more planar relative to the polyene backbone [70,71].
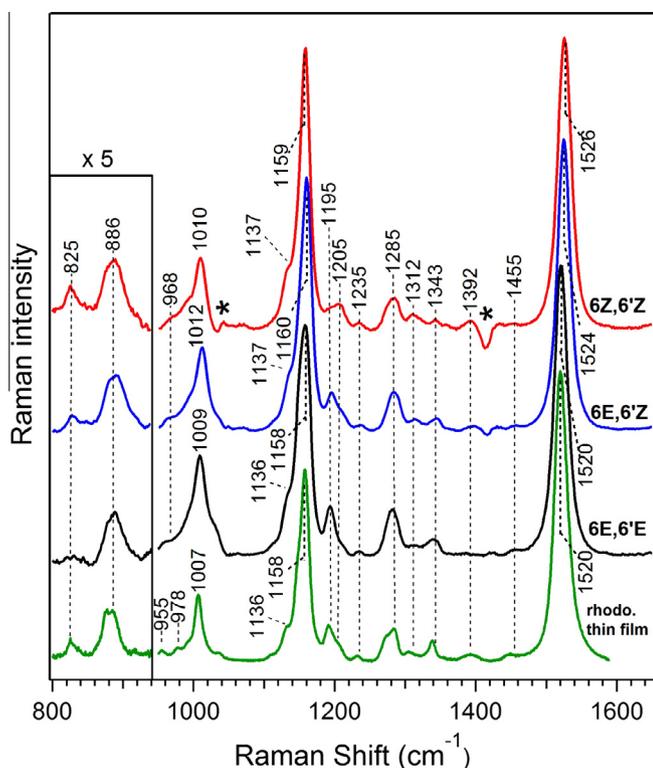
Fig. 8. Raman spectra of rhodoxanthin isomers (6Z,6'Z), (6E,6'Z), and (6E,6'E) in DMSO, and in solid state (thin film). The 800–950 cm^{-1} region is magnified 5×, and the spectra are normalized for equal amplitude of the ν_1 band. Raman spectra of rhodoxanthin in DMSO are acquired with excitation wavelength 568.2 nm. The asterisks (∗) denote regions where the solvent subtraction was imperfect. The thin film consists of (6E,6'E)-rhodoxanthin deposited on a glass substrate. The excitation wavelength was 514.5 nm, and the spectrum was acquired at relatively high irradiance levels with a Raman microscope. The spectra of thin films of the other isomers were nearly identical to the one shown here (see text and Supporting Information).

Fig. 9. Computed Raman spectra of three rhodoxanthin isomers, from DFT and normal-mode calculations. The frequency axis is scaled by 0.9614. The 800–980 cm^{-1} region is magnified by 50×. The intensities of the calculated spectra do not take into account any mechanism for resonance enhancement, and are therefore not expected to match the intensities of experimental resonance Raman spectra.

Some of the patterns in the intensities of the DFT calculations of the three isomers reflect trends seen in experiment. The agreement is perhaps fortuitous, given that the calculations only reflect the magnitude of the polarizability derivatives with respect to normal coordinate, whereas intensities in the experimental spectra depend upon mechanisms for resonance enhancement that are not considered in the calculations. For example, the intensities of a doublet in the 1385–1400 cm^{-1} region of the calculations can be compared with the experimental 1392 cm^{-1} band (strongest for the 6Z,6'Z isomer). The 1334/1335 cm^{-1} band in the calculations, which consists primarily of C13–C14 (C13'–C14') stretches with CH rocks, may reflect the experimental trend for the 1343 cm^{-1} band (strongest for 6E,6'E). A pair of bands in the calculations that are centered at 1181 cm^{-1} and 1194 cm^{-1} (strongest for 6E,6'E and 6Z,6'Z, respectively) can be compared with the relative intensities of the experimental bands at 1195 and 1205 cm^{-1} (strongest for 6E,6'E and 6Z,6'Z, respectively).

A number of other bands appear in the experimental spectra of rhodoxanthin, but are not in complete agreement with the off-resonance calculations. First and foremost, a band at ∼1135 cm^{-1} is a clear shoulder in the experimental spectra of all three rhodoxanthin isomers in solution, but is not apparent in the experimental spectrum of all-trans zeaxanthin. The calculations of rhodoxanthin reveal a normal mode with frequency in the range of 1137–1143 cm^{-1}, depending upon the isomer. The motion consists mainly of a localized C15–C15' stretch and accompanying CH rocks. Given that C15 and C15' are joined by a single bond for the retro-carotenoids, but double for the normal carotenoids, it is reasonable that a normal
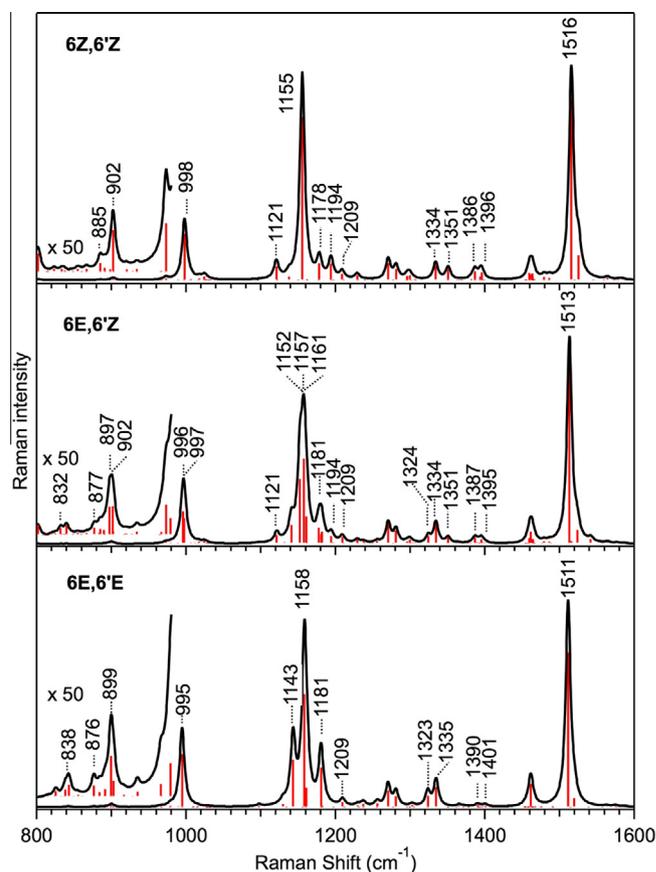
mode consisting primarily of this stretch could be a unique signature of the retro-carotenoids. The calculations suggest that the intensity of this band strongly depends on the isomer, in contradiction with the experimental spectra. A likely reason is that the polarizability changes computed in the off-resonance calculations include significant C–H rocking motion on the rings, and the net magnitude of the polarizability derivative (Raman intensity) is therefore sensitive to the isomeric form. In contrast, the resonance enhancement of the experimental band is likely derived from an A-term mechanism, i.e. Franck–Condon displacement along the C15–C15' stretching coordinate. Thus the actual mechanism for resonance enhancement is not expected to depend significantly upon local motions of the rings, or upon the configuration around the distant C6=C7 bond.

Second, the calculations predict a splitting of modes in the ν_2 region, corresponding to vibrations of both C–C single bond stretching and C–H rocking motions. A single strong band at 1155 cm^{-1} (6Z,6'Z) correlates with at least two bands centered at 1143 and 1158 cm^{-1} (for 6E,6'E). There is a hint of this trend in the experiment, because the ν_2 band in solution-phase spectra appears to be narrowest for (6Z,6'Z) and shows significant broadening for the (6E,6'E) isomer. Furthermore, the splitting seen in the calculations is similar to the splitting noted in the spectra of rhodoxanthin embedded in feathers (see below). However, the experimental solution-phase spectra of the reference samples were not sufficiently resolved to discern individual bands, thus it is not clear how the splitting or relative intensities of these two bands depends upon the isomer.

Table 3
Results from DFT calculations.

Molecule	E^a (cm^{-1})	Dihedral angle[b] (degrees)		Bond length (Å)		ν_1 (cm^{-1})
		D	D′	C6–C7	C6′–C7′	
(6E,6′E)-rhodoxanthin	+341	−179.9	−179.9	1.374	1.374	1511
(6E,6′Z)-rhodoxanthin	+177	176.8	160.1	1.374	1.370	1513
(6Z,6′Z)-rhodoxanthin	0	−160.1	160.1	1.370	1.370	1516
β-carotene	–	−48.9	48.9	1.475	1.475	1520
(6E,6′E)-isocarotene	–	−168.0	168.0	1.372	1.372	1518

[a] Optimized energy relative to (6Z,6′Z)-rhodoxanthin.
[b] The dihedral angles are C5=C6–C7=C8 for β-carotene, and C4=C5–C6=C7 for the retro-carotenoids.

Third, a small band at ∼825 cm^{-1} in the solution phase spectra of rhodoxanthin gains intensity in the series (6E,6′E) → (6Z,6′Z). A likely assignment for this band is HOOP wags of hydrogens C8H, C11H (and C8′H, C11′H) which move in opposition to wags C10H, C12H (and C10′H, C12′H). The calculations predict the frequency of this normal mode to be in the range 832–838 cm^{-1}, depending upon isomer, which is very close to the experimental value. Additionally, it is reasonable that a HOOP motion that is close to the C6=C7 or C6′=C7′ ends of the chromophore should be sensitive to the configuration at each end. However, the DFT results predict that the relative intensity of this mode is opposite the trend observed in the solution-phase spectra. Once again, the mismatch between the experimental and calculated relative intensities of this band likely results from the fact that resonance enhancement is not factored into the calculations and therefore they are generally not good predictors of the experimental intensities. To enhance support for the assignment it would be useful to include mechanisms for resonance enhancement in the calculations.

Resonance Raman spectra of rhodoxanthin thin films

A resonance Raman spectrum of a thin film of rhodoxanthin acquired with 514.5 nm excitation (high irradiance) is shown in Fig. 8. This film was formed from the (6E, 6′E) isomer, however films of the other isomers have band positions that are nearly indistinguishable from each other (see Figs. S4 and S5; Table S6). Specifically, the peak positions of all three isomers are ν_1 (1520–1521 cm^{-1}), ν_2 (1158 cm^{-1}), and ν_3 (1007 cm^{-1}). In addition, the HOOP region (800–980 cm^{-1}) shows no differentiation among isomers. Interestingly, the HOOP doublets at 955 and 978 cm^{-1} are more resolved than in the solution-phase spectra. As shown in Fig. S5, low temperature spectroscopy of the (6Z,6′Z) isomer exhibited the same spectra as at room temperature, although the ν_2 and ν_1 frequencies shifted 2–3 cm^{-1} higher. All bands were more resolved at low-temperature than room temperature, especially in the low-frequency and HOOP regions.

Given the nearly identical bands for the three thin films, it is possible that the same photoproduct or distribution of photoproducts forms by isomerization, regardless of the starting configuration. In support of this proposal, we note that a photolysis experiment of rhodoxanthin in solution reveals significant isomerization of a sample of pure (6E,6′Z)-rhodoxanthin into both (6E,6′E) and (6Z,6′Z) isomers upon irradiance with 488.0 nm laser excitation over the course of an hour (see Supporting Information and Fig. S6). More generally, a prior report showed that isomerization around the C6=C7 bond can take place at room temperature, particularly for the (6E,6′E) isomer, even in the absence of photolysis [72]. Despite what appears to be facile change in configuration, it should be noted that during the micro-Raman measurements of thin films, there were no qualitative changes in either the peak positions or in bandwidths at any point during the 15 min integration period. Therefore, if isomerization takes place upon excitation of the films, the equilibrium must be reached within the exposure

time of the first acquisition (30 s). Furthermore, even when the irradiance was decreased to levels at least 1000-fold lower than employed to acquire the spectrum of Fig. 8, there was no observable difference between the ν_1 peak positions of the (6E,6′E) and (6E,6′Z) isomers. It is possible that the quantum yield for isomerization is sufficiently high so that either level of irradiance causes the rhodoxanthin at the laser focus to reach isomeric equilibrium within the exposure time of the first acquisition. A less probable explanation is that the vibrational signatures of the three isomers, although significantly different in solution, are indistinguishable in thin films. There was insufficient rhodoxanthin to perform a HPLC/UV–Vis analysis following photolysis of the thin films of pure rhodoxanthin.

Raman spectra were previously reported for three red carotenoids extracted from *Potamogeton crispus* [42]. The three carotenoids were identified in a separate study as isomers of rhodoxanthin [43]. The authors indicated a peak maximum for the main ethylenic band at 1527 cm^{-1} for all three red carotenoids; this value is nearly identical to 1526 cm^{-1} that we find for the (6Z,6′Z) isomer. Furthermore, a weak band centered at ∼1395–1398 cm^{-1} was reported in the spectra of the unknown isomers of the red carotenoids [42]. This band nearly coincides with a minor one centered at ∼1392 cm^{-1} that is most distinct in our solution-phase spectrum of (6Z,6′Z)-rhodoxanthin. In considering both of these points, we conclude that isomerization affected the previous resonance Raman spectra [42] in a similar way that it probably affected the thin film results of the present study.

Resonance Raman spectra of rhodoxanthin-containing feathers

The room and low temperature resonance Raman spectra of the feathers are shown in Fig. 10. The 8 cm^{-1} variation in the peak maxima of ν_1 in the room temperature spectra of the feathers is slightly greater than the variation caused by various isomers of rhodoxanthin in solution. In the fingerprint region, there generally is a larger number of well-defined bands for the feathers than for the solution-phase spectra. For example, in the ν_2 region the feathers have significant Raman scattering in two main bands that are near 1159 and 1146 cm^{-1}, as well as a shoulder at ∼1132 cm^{-1}. The ν_2 region of rhodoxanthin in solution exhibits a single broad peak at ∼1159 cm^{-1}, with a shoulder at ∼1135 cm^{-1}. Like the solution phase spectra, the feathers have two small bands with peaks near 1195 and 1205 cm^{-1}, a pair of bands that are found at approximately 1275–1285 cm^{-1}, and there is a small band centered at ∼1342 cm^{-1}.

A comparison of the Raman spectra of the feathers at room temperature, with the solution-phase results suggests that the isomeric content of rhodoxanthin in the feathers is mixed. On one hand the intensity of the 1342 cm^{-1} band in the spectra of the feathers is most consistent with a predominantly (6E,6′E) or (6E,6′Z) configuration. Similarly, the overall shape of the bands near 1195 cm^{-1} most closely resemble the (6E,6′E) or (6E,6′Z) configurations in solution. However, the 1392 cm^{-1} band, which is
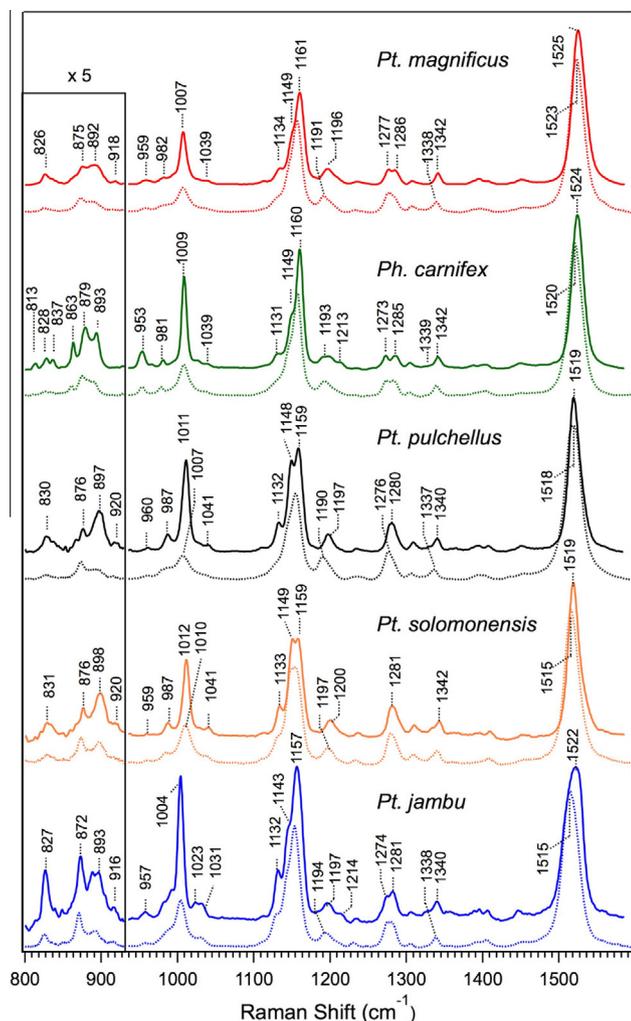
Fig. 10. Resonance Raman spectra of avian feathers acquired with 514.5 nm excitation and a microscope setup. The solid lines are spectra acquired at approximately −195 °C, and the dotted lines are those acquired at room temperature. The 800–930 cm^{-1} region is magnified by a factor of 5.

most clearly observed in the (6Z,6′Z) isomer, is observed in all five samples. The prominent Raman signals at ~830 cm^{-1}, also observed in each of the feather spectra, could support the presence of the Z configuration. Based on these comparisons, it is possible that the feathers contain a majority of molecules with the (6E,6′Z) configuration. However an inhomogeneous mixture of (6E,6′E) and (6Z,6′Z) isomers could also yield spectra that have a similar appearance. As noted for the thin films and in solution, it is possible that photoisomerization about the C6=C7 (C6′=C7′) bond of rhodoxanthin occurs in the feathers, and that a steady-state equilibrium of configurations is reached shortly after laser excitation begins. One way to assess whether an isomeric mixture is native in the feathers, or an artifact of excitation, would involve extraction of the chromophore without heat [4,39] (to preserve the native distribution of isomers), followed by HPLC analysis of the pigments.

Differences in the isomeric content among the feathers cannot be the sole cause of the variation in their absorption spectra. The shift of the absorption maxima between (6Z,6′Z)- and (6E,6′E)-rhodoxanthin is less than 500 cm^{-1}, whereas the estimated differences in the absorption spectra of the five feathers is ~1400 cm^{-1}.

In general, band frequencies increase slightly upon lowering the sample temperature. The bands clustered in the region of v_2 are better resolved at low-temperature. Additionally, the relative amplitudes of the low-frequency bands, as well as v_2 and v_3, tend to increase at low temperature, as compared with the v_1 band. The peak positions of the feather spectra at low-temperature and room temperature are summarized in Table S7.

Description of Raman spectra of individual feather samples

Pt. magnificus

This feather is characterized by the highest frequency for v_1 at 1525 (1523) cm^{-1} at low (room) temperature. The band is somewhat broadened relative to other samples, and only *Pt. jambu* has greater breadth. The v_2 region of *Pt. magnificus* is also broadened relative to others. The HOOP bands have the lowest intensities and are the least well resolved among all feathers. Most of the intensity in the HOOP region is found in the 875 and 892 cm^{-1} bands.

Ph. carnifex

This spectrum is most similar to *Pt. magnificus*. At low temperature, the v_1 band has its peak at 1524 cm^{-1}, only one wavenumber lower than the corresponding peak of *Pt. magnificus*. The maxima of the bands in the fingerprint region for both samples have frequencies that match one another within several wavenumbers. However, the spectra of *Ph. carnifex* appear to be the most well-resolved, with narrower v_2 and v_3 bands relative to spectra of *Pt. magnificus* and other species. Other bands in the fingerprint region, e.g. at 1273 and 1285 cm^{-1} are distinguishable even at room temperature. Likewise, the bands in the HOOP region are more resolved and numerous than for other feathers at low temperature. Unique to the Raman spectra of *Ph. carnifex* is a sharp mode at 863 cm^{-1}, and the intensity of the 953 cm^{-1} band is considerably greater than corresponding modes in the 950–960 cm^{-1} region of any other sample.

Pt. pulchellus and Pt. solomonensis

The low-temperature resonance Raman spectra of these feathers appear to have no significant differences. The v_1 frequency maxima (1519 cm^{-1}) are identical at low temperature. The fingerprint region reveals a band-for-band match for the two species, with at most a ~3 cm^{-1} difference in the position of corresponding maxima. Both show clear doublet character to v_2, with significant intensity of one band centered at 1148–1149 cm^{-1}, and another centered at 1159 cm^{-1}. A clear shoulder has a maximum at 1132–1133 cm^{-1}. Finally, the methyl rock and six HOOP modes match with at most 1 cm^{-1} difference in the positions of the maxima. The intensities of the HOOP modes are very similar in the spectra of the two feathers.

Pt. jambu

The ~7 cm^{-1} upshift in v_1 upon cooling (from 1515 to 1522 cm^{-1}) is a considerably greater change than seen for any other feather. The reason for the shift, as well as the overall greater breadth of this band is clear from the low-temperature spectrum, where it is obvious that the intensity in the v_1 region is due to two overlapping bands. A fit of the spectra to two Voigt profiles yields peak positions at 1510 cm^{-1} (small) and 1524 cm^{-1} (large). Another unusual aspect of the *Pt. jambu* resonance Raman spectrum is the anomalously large HOOP band at 827 cm^{-1}. The relative intensity in the HOOP mode region is greatest for *Pt. jambu* among all the samples.

Effect of irradiance on the resonance Raman spectra

A comparison of the low and high irradiance Raman spectra of the feathers is illustrated in Fig. S7. The high-irradiance experiments employed a tightly focused ~1 μm diameter beam that

could probe a specific area of a single barbule, whereas similar specificity was not possible for the 2.50 mm by 0.040 mm sized spot of the low-irradiance experiments. The irradiance levels of the micro-Raman experiments were 10^3–10^4 times higher than the macro-Raman experiments. Despite the differing areas and irradiance levels, the spectra are nearly identical. In some cases there are differences in peak positions of ~2 cm^{-1}. It is not clear whether these shifts are a consequence of the irradiance, or uncertainties in the wavelength calibration for the different experiments. The near-identical Raman spectra of carotenoids in feathers at high and low irradiance is consistent with a previous report [41].

Connections between electronic and vibrational spectroscopy

The origins of the vibrational and electronic changes of carotenoids in different environments have been addressed extensively for the caroteno-proteins of lobsters and other invertebrates [23,73] and carotenoid-containing feathers of birds [4,5,41]. We will discuss the results described above in the context of three mechanisms: (1) extent of conjugation, particularly the effects of distortion; (2) polarization of the chromophore via interaction with its environment; and (3) electronic coupling between carotenoids.

It is well known that an increase in the extent of conjugation (increase in π-electron delocalization) in a polyene system decreases both the energy of the HOMO–LUMO transition as well as the frequency of the ν_1 mode [74,75]. Is a change in the extent of conjugation, as reflected by the frequency of the ν_1 mode of rhodoxanthin in the feathers, consistent with the shifts in electronic absorption of the chromophore? The positions of the average half-maxima in the absorption are 20,100, 19,800, 19,200, and 18,700 cm^{-1} for *Pt. magnificus*, *Ph. carnifex*, *Pt. pulchellus*, and *Pt. solomonensis*, respectively. Resonance Raman spectra acquired at the same (room) temperature as the absorption spectra have peak maxima for the ethylenic frequencies at 1523, 1520, 1518, and 1515 cm^{-1}. (*Pt. jambu* is not considered in this analysis because of the complicating factor of two bands observed in the low-temperature Raman spectra.) A plot of the electronic energy versus ethylenic vibrational frequency yields a slope of nearly 200 cm^{-1} (change in electronic energy) per 1 cm^{-1} (change in vibrational frequency). By comparison, reports of the same correlation as a function of polyene length reveal a slope of ~95–120 cm^{-1} (electronic) per 1 cm^{-1} (vibrational) [74–76]. The electronic spectrum of rhodoxanthin changes more than one would expect from the variation in the ν_1 ground-state frequency. Additionally, changes in conjugation length are expected to affect both ν_1 and ν_2 frequencies [41,74,75]. The near-invariant frequency positions of strong bands in the ν_2 region of the feather spectra are one argument against differences in ground-state delocalization. Taken together, the preceding observations lead to the conclusion that changes in the absorption band of rhodoxanthin within the environment of the five feather samples are primarily a consequence of shifts in the excited-state energy level of the carotenoid, and secondarily a result of delocalization in the ground state.

The effective conjugation length of a polyene depends upon its planarity. One measure of loss in planarity is the enhanced Raman scattering from HOOP wags. These normal modes become fully symmetric, and therefore gain Raman intensity via the A-term, when the polyene is twisted [68,77]. For rhodoxanthin in the five feathers, the HOOP bands of the room-temperature spectra are slightly more intense when the ν_1 frequency is lowest. We would expect the opposite behavior: a low intensity of a HOOP band (sign of a flattened chromophore) should be connected to a downshifted ethylenic frequency (indicator of delocalization). Our view agrees with others [74,78]. However, there have been contrary claims that twisting around single or double bonds of the chromophore would cause a decrease in ν_1 ethylenic frequency [23]. Although we question the basis of the latter correlation, nevertheless, it matches the trend of our experimental spectra.

A polarization mechanism, e.g. one resulting from a hydrogen bond to a keto group, or the interaction of a nearby charge with the conjugated double bond network, can alter the electronic structure of the carotenoid in two ways. First, the presence of a charged residue near the polyene chain or conjugated carbonyl could decrease the extent of double- and single-bond alternation, effectively extending the conjugation. This mechanism should have a significant effect on the ground state, as well as the energy of the electronic transition [79]. Second, a nearby charged residue could perturb the excited state, while leaving the ground state largely unmodified. This alternative scenario is reasonable, in part because the carotenoid in its S_2 excited state is more polarizable than in the ground state [80]. Furthermore, particularly for a keto-carotenoid, any asymmetry in the interactions at either end of the chromophore can be expected to induce significant charge-transfer, and therefore a dipole moment, upon excitation. Charge transfer is one mechanism whereby the environment could shift the energy level of the excited state substantially, while the ground state is left relatively unperturbed. A similar model of excited-state perturbation was invoked to explain the green-to-red opsin shift of the visual pigment rhodopsin, which contains the chromophore 11-*cis* retinal [81].

Some degree of polarization of the ground-state rhodoxanthin in the feathers may be indicated by C=O stretching frequencies that are lower (~10 cm^{-1}) versus in the solution phase (Fig. S7). The decreased frequency could be caused by hydrogen bonding of an amino acid residue to a carbonyl. However, the decrease in frequency is significantly smaller than the typical 40–60 cm^{-1} downshifts for other hydrogen-bonded carbonyls [82]. The minor decrease in carbonyl frequency seen in our experimental spectra does not support strong hydrogen-bonding as the primary mechanism for polarization in the feathers. Again, we conclude that the evidence points to minimal perturbation of the ground-state chromophore, as part of the shift in the electronic transition.

Electronic coupling between neighboring carotenoid molecules may also perturb their excited-state energy levels. Exciton-coupling between astaxanthin molecules in crustacyanin was hypothesized to cause shifts in the absorption profile [13,14,22,83]. Although exciton-coupling shifts the excited state of the carotenoid, the ground state is unperturbed, thus leaving the vibrational frequencies the same [52,84]. In the case of the feathers, changes in the absorption profile, with only modest changes in the ν_1 frequency, may be indirect indicators that exciton coupling plays a role in the electronic transition of rhodoxanthin. Specifically, the downshifted electronic absorption of *Pt. pulchellus*, *Pt. solomonensis*, and *Pt. jambu* could be partially caused by chromophore–chromophore interaction. If this proposal is correct, the mechanism for bringing the chromophores close to one another must overcome the relatively low concentrations of rhodoxanthin in the feathers with the most red-shifted absorption bands (*Pt. solomonensis* and *Pt. jambu*).

Conclusions

In the present study, we have explored the variation of color in bird feathers that contain the retro-carotenoid rhodoxanthin. The plumage originates from four species of fruit doves (*Ptilinopus*) and a cotinga (Cotingidae). We analyzed the vibrational spectra of the retro-carotenoid, and identified bands and normal modes that distinguish it from more common carotenoids that have the usual pattern of single/double bond alternation.

Within the feathers of the five species, the shifts in ethylenic (v_1) band positions are inconsistent with the trend in HOOP wag intensities, and also cannot be reconciled with the ∼40 nm shift in the UV–Vis transition energy. Therefore, we propose that a polarization mechanism, or possibly exciton coupling between chromophores, exerts a particularly strong influence on the excited-state chromophore within the keratin environment. Shifts in the absorption of rhodoxanthin may be the primary cause of color variation, but other factors are not excluded. Eumelanin and pheomelanin in *Pt. magnificus*, *Pt. pulchellus*, *Ph. carnifex* could contribute to blue light absorption and enhance the feathers' overall red appearance, relative to those of *Pt. jambu* and *Pt. solomonensis*. It is also possible that structural coloration, or perhaps differences in carotenoid concentration, could affect the range of colors observed in the plumage of these birds.

Acknowledgments

Appendix A. Supplementary data

Supplementary data associated with this article can be found, in the online version, at http://dx.doi.org/10.1016/j.abb.2013.09.009.

References

[1] R.O. Prum, A.M. LaFountain, J. Berro, M.C. Stoddard, H.A. Frank, J. Comp. Physiol. B 182 (2012) 1095–1116.
[2] O. Völker, J. Ornithol. 94 (1953) 263–273.
[3] O. Völker, J. Ornithol. 102 (1961) 430–438.
[4] R. Stradi, G. Celentano, E. Rossi, G. Rovati, M. Pastore, Comp. Biochem. Physiol. B Biochem. Mol. Biol. 110B (1995) 131–143.
[5] M. Mendes-Pinto, A.M. LaFountain, M.C. Stoddard, R.O. Prum, H.A. Frank, B. Robert, J. R. Soc. Interface (2012) 3338–3350.
[6] H.W. Yin, L. Shi, J. Sha, Y.Z. Li, Y.H. Qin, B.Q. Dong, S. Meyer, X.H. Liu, L. Zhao, J. Zi, Phys. Rev. E 74 (2006).
[7] L. D'Alba, V. Saranathan, J.A. Clarke, J.A. Vinther, R.O. Prum, M.D. Shawkey, Biol. Lett. 7 (2011) 543–546.
[8] V. Saranathan, J.D. Forster, H. Noh, S.F. Liew, S.G.J. Mochrie, H. Cao, E.R. Dufresne, R.O. Prum, J. R. Soc. Interface 9 (2012) 2563–2580.
[9] K.J. McGraw, R.J. Safran, K. Wakamatsu, Funct. Ecol. 19 (2005) 816–821.
[10] K.J. McGraw, Mechanics of melanin-based coloration, in: G.E. Hill, K.J. McGraw (Eds.), Bird Coloration: Mechanisms and Measurements, vol. I, Harvard University Press, Cambridge, MA, 2006, pp. 243–294.
[11] G. Britton, R.J. Weesie, D. Askin, J.D. Warburton, L. Gallardo-Guerrero, F.J. Jansen, J.H.M. de Groot, J. Lugtenburg, J.-P. Cornard, J.-C. Merlin, Pure Appl. Chem. 69 (1997) 2075–2084.
[12] P.F. Zagalsky, Acta Crystallogr. Sect. D Biol. Crystallogr. 59 (2003) 1529–1531.
[13] R.P. Ilagan, R.L. Christensen, T.W. Chapp, G.N. Gibson, T. Pascher, T. Polívka, H.A. Frank, J. Phys. Chem. A 109 (2005) 3120–3127.
[14] A.A.C. van Wijk, A. Spaans, N. Uzunbajakava, C. Otto, H.J.M. de Groot, J. Lugtenburg, F. Buda, J. Am. Chem. Soc. 127 (2005) 1438–1445.
[15] H. Rademaker, A.J. Hoff, R. van Grondelle, L.N.M. Duysens, Biochim. Biophys. Acta 592 (1980) 240–257.
[16] W.J. McGann, H.A. Frank, Biochim. Biophys. Acta 725 (1983) 178–189.
[17] C. Wang, M.J. Tauber, J. Am. Chem. Soc. 132 (2010) 13988–13991.
[18] C. Wang, D.E. Schlamadinger, V. Desai, M.J. Tauber, ChemPhysChem 12 (2011) 2891–2894.
[19] M.B. Smith, J. Michl, Chem. Rev. 110 (2010) 6891–6936.
[20] M.B. Smith, J. Michl, Annu. Rev. Phys. Chem. 64 (2013) 361–386.
[21] O. Völker, J. Ornithol. 93 (1952) 122–129.

[22] G. Britton, J.R. Helliwell, Carotenoid–protein interactions, in: G. Britton, S. Liaaen-Jensen, H. Pfander (Eds.), Carotenoids, vol. 4, Birkhäuser Verlag, Basel, 2008, pp. 99–117.
[23] P.F. Zagalsky, E.E. Eliopoulos, J.B.C. Findlay, Comp. Biochem. Physiol. B Biochem. Mol. Biol. 97 (1990) 1–18.
[24] G. Britton, S. Liaaen-Jensen, H. Pfander, Carotenoids Handbook, Birkhäuser Verlag, Basel, Boston, Berlin, 2004.
[25] R. Kuhn, H. Brockmann, Dtsch. Chem. Ges. 66 (1933) 828–841.
[26] P. Karrer, E. Jucker, Carotenoids, Elsevier, Amsterdam, 1950.
[27] P.J. Peterson, J. Exp. Bot. 14 (1963) 1–9.
[28] M. Cyronak, G. Britton, K.L. Simpson, Phytochemistry 16 (1977) 612–613.
[29] K. Ida, F. Saito, S. Takeda, Bot. Mag. Tokyo 104 (1991) 157–169.
[30] H.G. Weger, S.N. Silim, R.D. Guy, Plant Cell Environ. 16 (1993) 711–717.
[31] Q. Han, K. Shinohara, Y. Kakubari, Y. Mukai, Plant Cell Environ. 26 (2003) 715–723.
[32] M. Merzlyak, A. Solovchenko, S. Pogosyan, Photochem. Photobiol. Sci. 4 (2005) 333–340.
[33] K. Hormaetxe, J.M. Becerril, I. Fleck, M. Pintó, J.I. García-Plazaola, J. Exp. Bot. 56 (2005) 2629–2636.
[34] A. Solovchenko, Stress-induced buildup of screening pigments, in: Photoprotection in: Plants, Springer-Verlag, Berlin Heidelberg, 2010.
[35] B. Czeczuga, B.D. Ryan, R.W. Spjut, J.-A.W. Flock, C.W. Beasley, R.E. Showman, R.D. Worthington, V.L. Boucher, Feddes Repertor. 108 (1997) 401–417.
[36] O. Völker, Naturwissenschaften 38 (1951). 565–565.
[37] J. Hudon, Can. J. Zool. Rev. Can. Zool. 69 (1991) 2311–2320.
[38] J. Hudon, M. Anciães, V. Bertacche, R. Stradi, Comp. Biochem. Physiol. B Biochem. Mol. Biol. 147 (2007) 402–411.
[39] J. Hudon, A. Storni, E. Pini, M. Anciães, R. Stradi, Auk 129 (2012) 491–499.
[40] M.M. Katsuyama, B. Jpn. Soc. Sci. Fish. 45 (1979) 1045.
[41] M. Veronelli, G. Zerbi, R. Stradi, J. Raman Spectrosc. 26 (1995) 683–692.
[42] H.-B. Wang, D.-D. Ren, L.-Z. Liu, J.-Y. Shi, Acta Hydrobiol. Sin. 28 (2004) 380–384.
[43] H. Wang, D. Ren, L. Liu, G. Peng, M. Zhang, S. Zhang, Sci. Agri. Sin. 37 (2004) 1363–1368.
[44] O. Isler, M. Montavon, R. Rüegg, P. Zeller, Helv. Chim. Acta 39 (1956) 454–462.
[45] H. Mayer, M. Montavon, R. Rüegg, O. Isler, Helv. Chim. Acta 50 (1967) 1606–1617.
[46] J.D. Surmatis, A. Walser, J. Gibas, Helv. Chim. Acta 53 (1970) 974–990.
[47] E. Widmer, R. Zell, H. Grass, R. Marbet, Helv. Chim. Acta 65 (1982) 958–967.
[48] E. Nicoară, V. Tămaș, G. Neamțu, C. Bodea, Liebigs Ann. Chem. 697 (1966) 201–203.
[49] H.H. Strain, M.R. Thomas, J.J. Katz, J. Org. Chem. 26 (1961) 5061–5064.
[50] B.C.L. Weedon, Spectroscopic methods for elucidating structures of carotenoids, in: L. Zechmeister (Ed.), Fortschritte der Chemie Organischer Naturstoffe, vol. 27, Springer-Verlag, Wien, 1969, pp. 81–130.
[51] T. Matsuno, M. Katsuyama, B. Jpn. Soc. Sci. Fish. 45 (1979) 1533–1538.
[52] C. Wang, C.J. Berg, C.-C. Hsu, B.A. Merrill, M.J. Tauber, J. Phys. Chem. B 116 (2012) 10617–10630.
[53] A.M. LaFountain, S. Kaligotla, S. Cawley, K.M. Riedl, S.J. Schwartz, H.A. Frank, R.O. Prum, Arch. Biochem. Biophys. 504 (2010) 142–153.
[54] K.J. McGraw, J. Hudon, G.E. Hill, R.S. Parker, Behav. Ecol. Sociobiol. 57 (2005) 391–397.
[55] M.J.T. Frisch, G.W. Schlegel, H.B. Scuseria, G.E. Robb, M.A. Cheeseman, J.R. Scalmani, G. Barone, V. Mennucci, B. Petersson, G.A. Nakatsuji, H. Caricato, M. Li, X. Hratchian, H.P. Izmaylov, A.F. Bloino, J. Zheng, G. Sonnenberg, J.L. Hada, M. Ehara, M. Toyota, K. Fukuda, R. Hasegawa, J. Ishida, M. Nakajima, T. Honda, Y. Kitao, O. Nakai, H. Vreven, T. Montgomery Jr., J.A. Peralta, J.E. Ogliaro, F. Bearpark, M. Heyd, J.J. Brothers, E. Kudin, K.N. Staroverov, V.N. Kobayashi, R. Normand, J. Raghavachari, K. Rendell, A. Burant, J.C. Iyengar, S.S. Tomasi, J. Cossi, M. Rega, N. Millam, J.M. Klene, M. Knox, J.E. Cross, J.B. Bakken, V. Adamo, C. Jaramillo, J. Gomperts, R. Stratmann, R.E. Yazyev, O. Austin, A.J. Cammi, R. Pomelli, C. Ochterski, J.W. Martin, R.L. Morokuma, K. Zakrzewski, V.G. Voth, G.A. Salvador, P. Dannenberg, J.J. Dapprich, S. Daniels, A.D. Farkas, Ö. Foresman, J.B. Ortiz, J.V. Cioslowski, D.J. Fox, Gaussian 09, Gaussian, Inc., Wallingford, CT, 2009.
[56] C.J. Cramer, Essentials of Computational Chemistry: Theories and Models, John Wiley & Sons Ltd., West Sussex, 2002.
[57] S. Andersson, M. Prager, E.I.A. Johansson, Funct. Ecol. 21 (2007) 272–281.
[58] J. Hudon, G.F. Grether, D.F. Millie, Physiol. Biochem. Zool. 76 (2003) 776–790.
[59] G.B. Cordon, M. Gabriela Lagorio, J. Chem. Ed. 84 (2007) 1167–1170.
[60] K.R. Millington, Amino Acids 43 (2012) 1277–1285.
[61] P. Meredith, T. Sarna, Pigm. Cell Res. 19 (2006) 572–594.
[62] J. Dyck, Structure and light reflection of green feathers of fruit doves (*Ptilinopus* spp.) and an Imperial Pigeon (*Ducula concinna*), in: Biologiske Skrifter, Copenhagen, Royal Danish Academy of Sciences and Letters, 1987, pp. 2–43.
[63] R.O. Prum, Anatomy, physics, and evolution of avian structural colors, in: G.E. Hill, K.J. McGraw (Eds.), Bird Coloration: Mechanisms and Measurements, vol. 1, Harvard University Press, Cambridge, MA, 2006.
[64] S. Saito, M. Tasumi, J. Raman Spectrosc. 14 (1983) 310–321.
[65] Y. Koyama, Resonance Raman spectroscopy, in: G. Britton, S. Liaaen-Jensen, H. Pfander (Eds.), Carotenoids: Spectroscopy, vol. 1B, Birkhäuser Verlag, Basel, Boston, Berlin, 1995.
[66] B. Robert, The electronic structure, stereochemistry and resonance Raman spectroscopy of carotenoids, in: H.A. Frank, A.J. Young, G. Britton, R.J. Cogdell (Eds.), Advances in Photosynthesis, Photochemistry of Carotenoids, vol. 8, Springer, 1999, pp. 189–201.

[67] N. Tschirner, M. Schenderlein, K. Brose, E. Schlodder, M.A. Mroginski, P. Hildebrandt, C. Thomsen, Status Solidi. B Basic Solid State Phys. 245 (2008) 2225–2228.
[68] G. Eyring, B. Curry, A. Broek, J. Lugtenburg, R. Mathies, Biochemistry 21 (1982) 384–393.
[69] I. Palings, E.M.M. van den Berg, J. Lugtenburg, R.A. Mathies, Biochemistry 28 (1989) 1498–1507.
[70] L. Zechmeister, Cis-Trans Isomeric Carotenoids Vitamins A and Arylpolyenes, Springer-Verlag, Vienna, 1962.
[71] J. Dale, Acta Chem. Scand. 8 (1954) 1235–1256.
[72] G. Englert, M. Vecchi, J. Chromatogr. 235 (1982) 197–203.
[73] M. Buchwald, W.P. Jencks, Biochemistry 7 (1968) 844.
[74] J.C. Merlin, J. Raman Spectrosc. 18 (1987) 519–523.
[75] L. Rimai, M.E. Heyde, D. Gill, J. Am. Chem. Soc. 95 (1973) 4493–4501.
[76] H.E. Schaffer, R.R. Chance, R.J. Silbey, K. Knoll, R.R. Schrock, J. Chem. Phys. 94 (1991) 4161–4170.
[77] B. Robert, Photosynth. Res. 101 (2009) 147–155.
[78] V.R. Salares, N.M. Young, H.J. Bernstein, P.R. Carey, Biochim. Biophys. Acta 576 (1979) 176–191.
[79] B. Durbeej, L.A. Eriksson, Chem. Phys. Lett. 375 (2003) 30–38.
[80] S. Krawczyk, G. Britton, Biochim. Biophys. Acta Protein Struct. Mol. Enzy. 1544 (2001) 301–310.
[81] G.G. Kochendoerfer, S.W. Lin, T.P. Sakmar, R.A. Mathies, TIBS 24 (1999) 300–305.
[82] G. Socrates, Infrared and Raman Characteristic Group Frequencies: Tables and Charts, Wiley Chichester, UK, 2001.
[83] A. Strambi, B. Durbeej, J. Phys. Chem. B 113 (2009) 5311–5317.
[84] V.R. Salares, N.M. Young, P.R. Carey, H.J. Bernstein, J. Raman Spectrosc. 6 (1977) 282–288.